Desalination and Water Treatment
www.deswater.com

doi: 10.5004/dwt.2017.20726

74 (2017) 96–104
May

Effect of MPD concentration in the coagulation bath on the performance of CTA flat-sheet FO membrane fabricated by CTA–NMP–TMC casting solution

Xue-Jiao Guo†, Ping-Yun Zhang†, Xiang-Yu Chi, Zhen-Liang Xu*, Yong-Di Liu

State Key Laboratory of Chemical Engineering, Membrane Science and Engineering R&D Lab, Chemical Engineering Research Center, East China University of Science and Technology, 130 Meilong Road, Shanghai 200237, China, Tel. +86-21-64253670; Fax: +86-21-64252989; emails: chemxuzl@ecust.edu.cn (Z.-L. Xu), 1442773036@qq.com (X.-J. Guo), muyige988122@163.com (P.-Y. Zhang), chemchixy@foxmail.com (X.-Y. Chi), ydliu@ecust.edu.cn (Y.-D. Liu)

Received 19 September 2016; Accepted 21 March 2017

ABSTRACT

In situ interfacial polymerization method was utilized to fabricate cellulose triacetate (CTA) forward osmosis (FO) flat-sheet membrane using CTA–*N*-methyl-2-pyrrolidone (NMP)–trimesoyl chloride (TMC) casting solution, non-woven fabric as the support layer and *m*-phenylenediamine (MPD) aqueous solution as the coagulation bath. It is believed that interfacial polymerization occurred synchronously with the precipitation process of the casting solution. On the one hand, the interfacial polymerization occurred on the both surfaces of the CTA's top and bottom; on the other hand, the in situ interfacial polymerization resulted in the polyamide selective separation layer throughout the whole bulk of resultant CTA FO membranes. One of the interesting results was that the permeability properties of FO and pressure retarded osmosis mode improved in terms of increased pure water flux and decreased reverse salt flux as the increasing concentration of the MPD in the coagulant. Besides, the permeability difference between the two modes was tiny. The other novel result was that the increased MPD concentration of the coagulant contributed to the decreased *S* value. In addition, the resultant CTA membranes had excellent rejection and improved hydrophilicity.

Keywords: Cellulose triacetate; Forward osmosis membranes; In situ polymerization

1. Introduction

With the population drastically growing and the oil reserves rapidly depleted in twentieth century, water and energy consumption is increasing at a tremendous rate. Thus, water shortage and energy crises have been a serious issue all over the world [1–3]. Membrane separation technology plays a more crucial role in water treatment area in recent years. The membrane process especially reverse osmosis (RO) and nanofiltration (NF) has been an emerging and effective technology to obtain drinkable water. Nowadays, forward osmosis (FO) becomes a promising technology grabbing increasing attention [4,5]. Unlike pressure-driven membranes, it takes use of osmotic pressure gradient between the feed solution and draw solution instead of hydraulic pressure to drive water permeation through the semi-permeable membranes. It consumes significantly less energy and more resistant to membrane fouling, and the operation cost is lower [6–8]. However, the lack of high performance FO membranes impedes the large-scale application of FO technology in industry [9–11].

For the past few years, cellulose acetate (CA) becomes a preferential FO membrane material [12–15]. It is excellent for numerous distinct advantages including readily availability, high chloride resistance, good mechanical strength and excellent biocompatibility, and it has been a popular material to fabricate various membranes such as RO membranes [16–19], dialysis membranes [20–22], NF membranes [23] and ultrafiltration membranes [24]. Most importantly, CA's high hydrophilicity contributes to increasing

* Corresponding author.

† These authors contributed equally to this study.

water flux and decreasing membrane fouling propensity. Compared with CA, cellulose triacetate (CTA) is superior to chlorine resistance and exhibits much better hydrolytic stability. Therefore, it is a more preferential material to prepare FO membrane.

There are two main methods for fabrication of FO membranes: (a) non-solvent-induced phase inversion method for regular symmetry or asymmetry ones and (b) interfacial polymerization for thin-film composite (TFC) ones. As for the former, many researchers focus on the double-skinned FO membranes [25,26]. Reason behind that is the dense top and bottom surfaces enable to prevent the salt diffusion into the porous support layer thus mitigating the internal concentration polarization (ICP). Chung et al. [9] systematically explored the formation engineering and science of CTA FO membrane. It demonstrated that CTA polymer chain showed different interaction with different solvents thus resulting in different membrane structure. The CTA membrane processed denser bottom layer when using dioxane as solvent instead of NMP [27]. For the latter, the TFC membranes always possess a porous substrate and dense active layer [28–30]. The dense active layer is obtained via interfacial polymerization, whereas the porous substrate is the supportive layer. Using hydrophilic polyethersulfone (PES)/polysulfone (PSF) and cellulose ester as substrates, Chung's group prepared several TFC FO membranes [31–33]. The hydrophilic substrate is conducive to enhance FO performances. Nowadays, the popular porous support layer is nanofibers fabricated with electrospinning [34–37]. The highly interconnected pore structure and high porosity of the supportive layer contribute to significantly eliminate ICP [38,39]. Recently, modifying FO membranes with nanomaterials is another novel method to fabricate TFC FO membrane. The functional nanomaterial is directly grafted on surface of polyamide active layer or incorporated into the membrane substrate by blending method. The nanoparticles would affect membrane hydrophilicity, porosity and structural parameter (S), and improve membrane permeability performance [40]. The ocular interpretation of regular fabrication methods of FO membranes is exhibited in Fig. 1.

Considering the tedious steps of the TFC membranes' fabrication, one simplified method was used to fabricate FO membranes with dense selective layer and porous substrate. In our previous study, in situ interfacial polymerization was designed to prepare CTA FO membranes with the dense selective bottom surface, as well porous top surface and the substrate. The in situ interfacial polymerization was that the interfacial polymerization between the organic monomer of trimesoyl chloride (TMC) and the aqueous monomer of *m*-phenylenediamine (MPD) synchronously occurred with that of the demixing process, and its implementation steps of the in situ interfacial polymerization were as follows. First, the TMC was directly blended with CTA to form the casting solution. Then MPD aqueous solution was utilized as coagulation bath. And the CTA FO membranes were successfully fabricated after the precipitation process of the casting solution in the MPD coagulant. It is believed that the polyamide that synthesized via in situ interfacial polymerization worked as the selective layer thorough the whole porous substrate. However, the dense layer that formed on the glass plane side limited the further improvement of the FO permeability properties of resultant CTA membranes. In order to eliminate the dense layer, the non-woven fabric was utilized as support substrate. In this study, the membranes were casted on the non-woven fabric to inquire into the structure and performances changes. During the demixing process, the in situ interfacial polymerization synchronously occurred on the bottom and top surfaces of resultant CTA membranes. The influence of MPD concentration in the coagulant on the FO permeability properties, membrane morphology and contact angle was investigated.

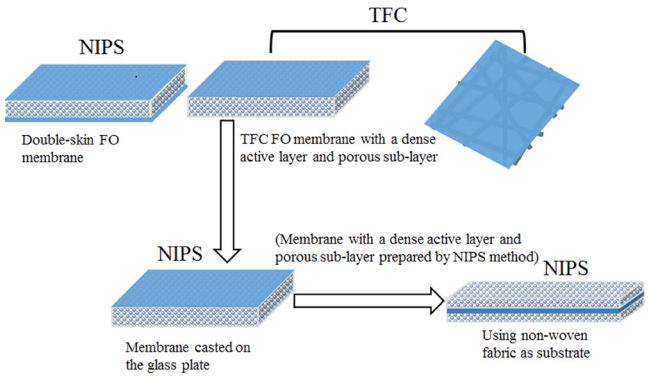

Fig. 1. Schematic diagram of different membrane structure.

2. Experimental

2.1. Materials

CTA (99.5%) polymer was purchased from Sino Polymer Co. Ltd., Shanghai, China. It should be stored in the 60°C vacuum oven overnight before using. *N*-methyl-2-pyrrolidone (NMP, 99.5%) and hexane were obtained from Merck and Shanghai Chemical Agent Co., Shanghai, China, respectively. TMC (≥98%) and MPD (>99%) were employed as monomers for polymerization, and they were obtained from Qingdao Benzo Chemical Company (China) and Sigma-Aldrich, Shanghai, China, respectively. Sodium chloride (NaCl) was draw solute to test membranes. It was purchased from Sinopharm Chemical Reagent Co. Ltd. (China). All these reagents were of analytical grade and were directly used without purification. Deionized (DI) water was provided by our own lab.

2.2. Preparation of CTA TFC FO membranes via in situ polymerization

13.0 wt% CTA was added in NMP at 60°C for at least 12 h to form the homogeneous solution. Then 0.1 wt% TMC dissolved in hexane was added into the above solution. Keep stirring at 60°C until the solution was homogeneous again. Finally, the solution was stored in a 60°C vacuum oven for 12 h to degas.

The membrane was prepared via in situ polymerization method using the non-woven as porous substrate. First, the non-woven was pasted onto a clean and smooth glass. Then the CTA casting solution was casted with a certain thickness casting knife, followed with immediate immersion into a certain concentration MPD aqueous solution for 2 min at ambient temperature. The MPD solution acted as coagulation bath to induce phase inversion and MPD reacted with

TMC to form the polyamide selective active layer simultaneously. After precipitation, the as-cast membranes were stored in DI water for 3 d to remove residual solvents. The detailed membrane fabrication conditions were summarized in Table 1. And the membranes fabrication process was shown in Fig. 2.

2.3. Characterizations of TFC FO membrane

2.3.1. Evaluation of FO permeability properties

The FO performances including the water flux and the salt reverse flux were tested in a lab-scale FO setup as depicted in Fig. 3. DI water and 1 M NaCl aqueous solution were used as feed solution and draw solution, respectively. Both of them were circulated with cross flow at ambient temperature. And the cross-flow velocity was 80 mL/min. All membranes were evaluated in FO mode (top surface faced feed solution) and pressure retarded osmosis (PRO) mode (bottom surface faced feed solution). And all the results were gained from three repeat experiments. The water flux was obtained from Eq. (1):

$$J_w = \frac{\Delta m / \rho}{A_m \Delta t} \tag{1}$$

where J_w is water flux (L/m²h, abbreviated as LMH); Δm represented the quality change of the feed solution in the predetermined time. ρ is the density of the feed solution (ρ_{water} = 1 g/cm³). A is effective membrane area 23.76 × 10⁻⁴ m², and Δt expresses the measuring time interval.

And reverse salt flux was calculated by using Eq. (2):

$$J_s = \frac{\Delta C_t V_t}{A_m \Delta t} \tag{2}$$

where J_s is salt reverse flux (g/m²h, abbreviated as gMH); C_t and V_t represent the salt concentration and volume of the feed solution at the end of the test, respectively. In this research, the salt concentration was obtained by measuring the solution conductivity; then, the salt concentration was calculated on the fitting curve of NaCl solution conductivity and concentration.

Table 1
The influence of MPD concentration

Membrane No.[a]	CTA (wt%)	NMP (wt%)	TMC (wt%)	MPD (wt%)
MCTA13-00	13	86.9		0.00
MCTA13-02	13	86.9		0.02
MCTA13-04	13	86.9		0.04
MCTA13-06	13	86.9	0.1	0.06
MCTA13-08	13	86.9		0.08
MCTA13-10	13	86.9		0.10
MCTA13-100	13	86.9		1.00

[a]The precipitation time of all membranes is 120 s.
Note: Thickness is 80 μm.

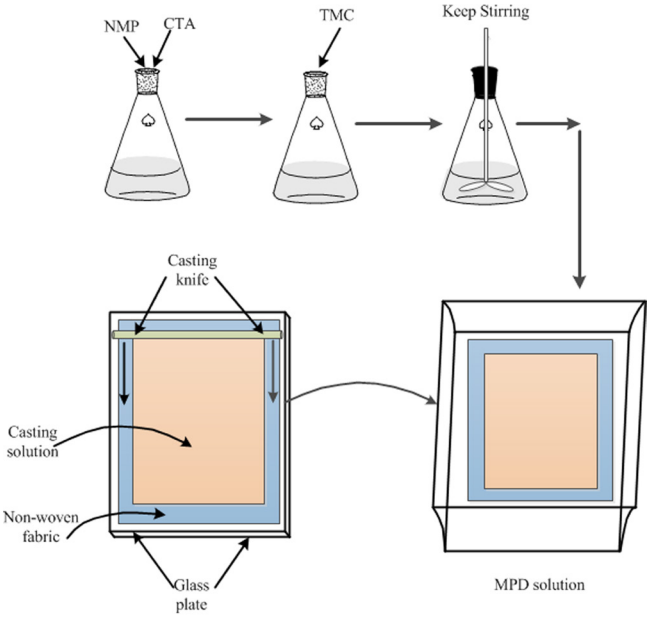

Fig. 2. The in situ interfacial polymerization method diagram for fabrication of CTA FO flat-sheet membranes using non-woven as supportive.

2.3.2. Membrane intrinsic separation properties

The pure water permeability coefficient A of resultant CTA flat-sheet FO membranes was measured in the RO mode by cross flow with applied pressure being 1 bar. And A was measured by using DI as feed solution, and it was obtained from Eq. (3):

$$A = \frac{J_v}{\Delta P} \tag{3}$$

where ΔP presented the applied pressure, and pure water volume flux J_v was obtained by measuring the volume of the permeation water during a predetermined time.

The salt permeability coefficient B was obtained in PRO mode. Using 1,000 ppm NaCl and DI as draw solution and feed solution, respectively. And B was gained by using Eq. (4) [41]:

$$B = \frac{1}{A_m t\left(\frac{1}{V_{draw}} + \frac{1}{V_{feed}}\right)} \ln\left(\frac{C^0_{draw} - C^0_{feed}}{C^t_{draw} - C^t_{feed}}\right) \tag{4}$$

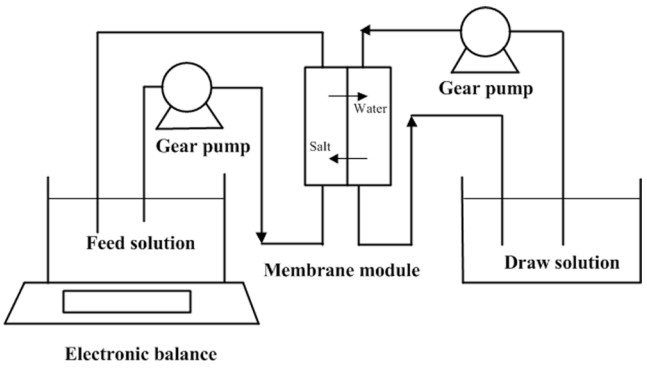

Fig. 3. The lab-scale FO test setup.

where A_m represents effective membrane area 23.76 × 10^{-4} m^2; V_{draw} and V_{feed} are the volume of the draw and the feed solution, respectively. The concentration of NaCl in the draw (C_{draw}) and feed (C_{feed}) were obtained by measuring the solution conductivity.

The salt rejection (R) was obtained from FO performance characterization by using Eq. (5) [42]:

$$R = \left(1 - \frac{C_{ft} - C_{f0}}{C_{Ds0}}\right) * 100 \quad (5)$$

where R denotes the salt rejection, and C_{Ds0} is the salt concentration in the initial draw solution; C_{f0} and C_{ft} are the salt concentration of the feed solution at the beginning and the end of the test, respectively.

S was acquired from the FO testing experiment in the PRO mode. Then it was obtained based on Eq. (6) [41]:

$$S = \frac{D}{J_w} \ln \frac{B + A\pi_{D,b} - J_w}{B + A\pi_{F,b}} \quad (6)$$

where D was the salt diffusion coefficient, and it was 1.61 × 10^{-9} m^2/s for NaCl. $\pi_{D,b}$ and $\pi_{F,b}$ signified the osmotic pressure of draw solution and feed solution, respectively. In this research, the osmotic pressure of 1 M NaCl draw solution was 4.74 MPa.

The porosity (ε) of CTA flat-sheet FO membranes was determined by dry-wet weight method. Remove the water on the membrane surface by tissue paper and obtain the weight of wet membrane m_1. Then wet membrane was stored in the 60°C dry oven for 24 h to obtain the weight of dry membrane m_2. The porosity was finally calculated by using Eq. (7):

$$\varepsilon = \frac{\frac{m_1 - m_2}{\rho_{H_2O}}}{\frac{m_1 - m_2}{\rho_{H_2O}} + \frac{m_2}{\rho_p}} \quad (7)$$

where ρ_{H_2O} is the density of water, 1.0 g/cm^3, and ρ_p is the density of CTA, 1.33 g/cm^3.

2.3.3. Dynamic contact angle (DCA)

To obtain the membrane hydrophilicity, the pure water DCA of membrane top surface was measured with a contact angle machine (JC2000A, Shanghai Zhongcheng Digital Equipment Co., Ltd., China) at ambient temperature. First, the samples were pasted onto the glass slide. Then disperse a water droplet of about 0.2 μL on the membrane top surface. The picture would be captured by the machine connected with the camera. And the contact angle was finally obtained via the specific calculation software. Each membrane was tested 3 times, and the average results were taken.

2.3.4. Field-emission scanning electronic microscopy (FESEM)

The membranes surface morphology was characterized by FESEM (S-4800, HI-9054-0006). The membranes were first immersed into liquid nitrogen and fractured. Then, all samples were sprayed with a thin gold layer for 60 s. The morphology of the top surface and cross section were obtained.

2.3.5. Atomic force microscope (AFM)

The surface roughness of resultant CTA FO membranes was characterized by AFM (Veeco, Nanoscope IIIa Multimode AFM). Then use the NanoScope Analysis software to obtain the membrane surface roughness including the root mean square roughness (Rms) and the mean roughness (Ra).

2.3.6. Energy-dispersive spectrometer (EDS)

EDS (Falcon, EDAX Inc., USA) was adopted to analyze the elemental composition mainly the oxygen, carbon and nitrogen mass ration of top surface of CTA FO membranes.

2.3.7. X-ray photoelectron spectroscopy (XPS)

Surface chemical composition of CTA FO membrane was further analyzed by XPS.

3. Results and discussion

3.1. Characterization of CTA membranes prepared via in situ interfacial polymerization using non-woven as substrate

3.1.1. SEM analysis

Fig. 4(A) shows the SEM images of top surface of the CTA FO membranes fabricated from various concentrations of MPD coagulant at 50,000 magnifications. There were some obvious cracks on the top surfaces of those membranes. Observed in detail of Fig. 4(A), the wrinkles appeared with the existence of MPD in the coagulant. Besides, those

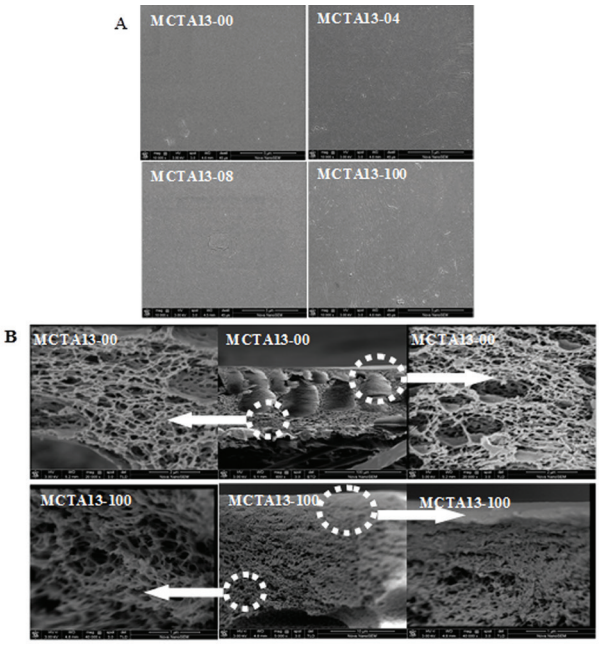

Fig. 4. SEM image of CTA membranes prepared via in situ interfacial polymerization using non-woven as substrate ((A) – top surface, (B) – cross section).

wrinkles were enhanced with increasing concentration of MPD in the coagulant. The reason for the formation of the wrinkles was the polymerization reaction of TMC and MPD on the membrane surface during demixing process. And the enhanced cracks came from the enlarged polyamide selective layer with increasing MPD concentration in the coagulants.

Fig. 4(B) is the SEM images of the cross section of CTA FO membrane prepared by using DI water and 1 M MPD as coagulation bath. It should be noted that all these membranes possessed a thin, dense skin layer and the porous sublayer. When DI water was coagulation bath, the membrane presented sponge-like structure near the both top surface and bottom surface with macrovoids between them. And the macrovoids were relatively closer to the top surface. When further magnified, it showed the highly porous network structure of the sub-layer. However, when MPD worked as the coagulation bath, the macrovoid structure disappeared, and the whole cross section of resultant CTA membrane was sponge-like structure. And the sub-layer was obviously less porous. It was ascribed to the polyamide active layer throughout the whole membrane bulk. Generally, macrovoids of the membrane tend to lead to high porosity. As is shown in Table 6, the CTA membrane presented the highest porosity when using DI water as coagulation bath, and the porosity decreased obviously as the MPD concentration increased in the coagulation bath.

3.1.2. AFM analysis

For the better understanding of membrane surface morphology, AFM was exploited to characterize the roughness of membrane top surface. Fig. 5 shows the AFM images of various CTA FO membranes, and the Rms and the Ra are summarized in the Table 2. Peak and valley structure was observed on the both membrane surface. Besides, both the Ra and the Rms increased remarkably with the increase of MPD concentration in the coagulation bath, which indicated the increasing roughness of membrane surface. It was attributed to the enlarged polyamide forming on the membrane surface as MPD concentration increased. However, the Ra of MCTA13-00 was little different from the Ra of MCTA13-10. The reason was that there was only 0.1 wt% TMC in the casting solution and little polyamide was formed. Furthermore, the rougher membrane surface was advantageous for the droplet to spread out so the contact angle decreased. This partly explained the decrease of DCA as increasing the MPD concentration in the coagulation bath. What's more, higher roughness led to larger membrane effective area, which was conductive to increase water flux.

3.1.3. EDS and XPS analysis

Besides the surface roughness, the contact angle of membrane was also influenced by the membrane composition. Therefore, the elemental composition of top surface of CTA FO membrane was further analyzed by EDS and XPS. XPS wide-scan spectra of CTA membranes are shown in Fig. 6. And the results are summed up in Tables 3 and 4, respectively. The existence of nitrogen element (N) exactly proved the formation of polyamide during the demixing process. Although the N content was remarkably varied when measured by EDS and XPS, the change rule remained same namely N content increased as MPD concentration in coagulation bath increased, which was the result of enhanced polyamide active layer. The different results in EDS and XPS were owing to the fact that the polyamide was throughout the whole membrane bulk, whereas EDS and XPS showed different scan depth. Namely the scan depth of XPS was only about 10 nm from membrane surface, whereas the scan depth of EDS was almost several micrometers. The different results exactly exhibited the separation of polyamide in the membrane bulk.

3.1.4. Dynamic water contact angle (DCA)

Fig. 7 exhibits the DCA of CTA membranes prepared from various MPD coagulants. It could be observed that both

Table 2
The roughness of CTA membranes prepared via in situ interfacial polymerization using non-woven as substrate

Membrane No.	Ra (nm)	Rms (nm)
MCTA13-00	2.97	85.6
MCTA13-10	2.92	55.3
MCTA13-100	3.43	88.8

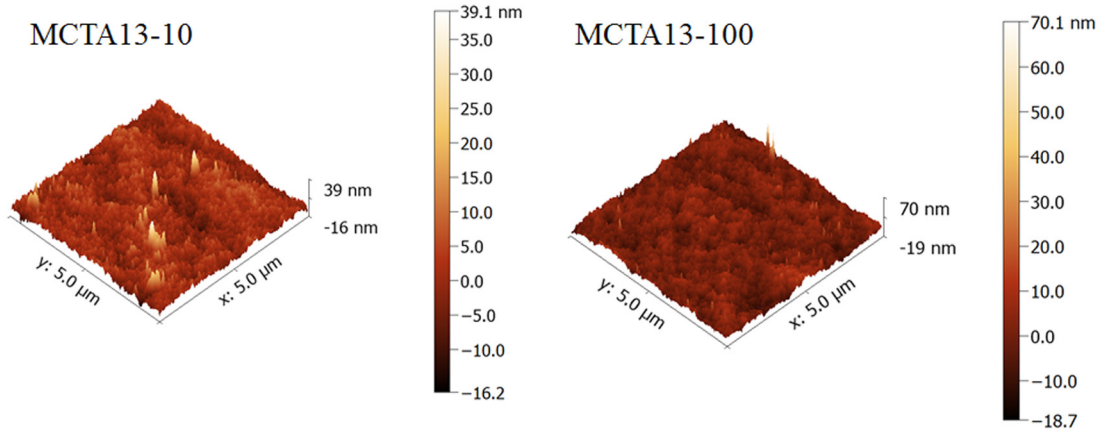

Fig. 5. AFM images of CTA membranes prepared via in situ interfacial polymerization using non-woven as substrate.

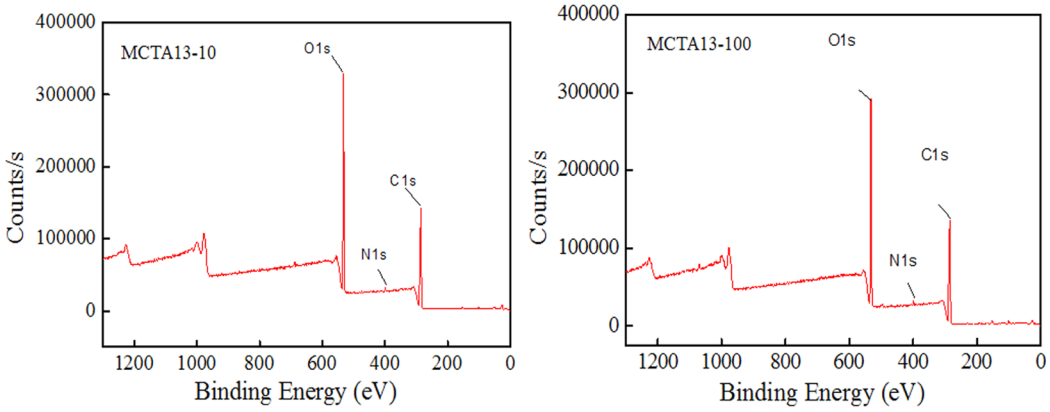

Fig. 6. XPS wide-scan spectra of CTA membranes prepared via in situ interfacial polymerization using non-woven as substrate.

Table 3
Elemental composition by EDS of top surface of CTA membranes prepared via in situ interfacial polymerization using non-woven as substrate

Membrane No.	C		O		N	
	wt%	Atom%	wt%	Atom%	wt%	Atom%
MCTA13-00	55.15	62.09	44.85	37.91	0	0
MCTA13-10	46.25	52.47	39.28	33.45	14.47	14.08
MCTA13-100	42.60	48.81	42.38	36.45	15.02	14.75

Table 4
Elemental composition by XPS of top surface of CTA membranes prepared via in situ interfacial polymerization using non-woven as substrate

Membrane No.	Atom%		
	C	O	N
MCTA13-10	59.45	37.95	1.04
MCTA13-100	61.01	35.45	1.45

the start contact angle and the equilibrium contact angle decreased as increasing concentration of MPD in the coagulants. Reason behind that could be the enlarged polyamide selective layer caused by the increased MPD. Besides, the curves indicated that the DCA significantly decreased with the measuring time increasing. It was the active layer of the porous structure that explained the decreased contact angle. And these results were well in accordance with the FO performance of resultant CTA membranes. Without MPD in the casting solution, MCTA13-00 had the lowest contact angles of the start and the equilibrium, reason for that could be the hydrophilicity of CTA was much better than that of polyamide formed on the membrane surface.

3.2. Evaluation of the FO and PRO modes' permeability properties of CTA membranes prepared via in situ interfacial polymerization using non-woven as substrate

3.2.1. Performance of CTA FO membranes

Table 5 displays the permeability properties of the FO and PRO mode of resultant CTA FO membranes. As the

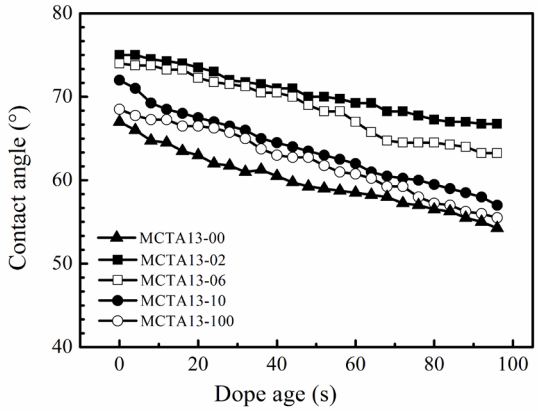

Fig. 7. Dynamic contact angles of CTA membranes prepared via in situ interfacial polymerization using non-woven as substrate.

results showed that with the increasing concentration of MPD in the coagulants, the water flux improved, and the reverse salt flux decreased. It is attributed to the fact that TMC in the casting solution reacted with the MPD in phase separation process forming the polyamide selective layer. And the selective layer enhanced when MPD concentration increased. This selective layer explained the improvement of the permeability properties of both FO and PRO mode. The reason for tiny differences between FO and PRO mode was the polyamide selective layer throughout the whole bulk of the resultant CTA membranes. Besides, the polyamide selective layer prevented the salt diffusion into the porous layer thus alleviating the ICP and increasing water flux.

Fig. 8 shows the NaCl rejection of CTA FO membranes fabricated from various MPD coagulants. It is obvious that the *R* increased when MPD existed in the coagulation bath. The reason was the polyamide selective layer formed during the demixing process. Besides, the *R* increased when MPD concentration increased. That was owing to the enhanced selective layer throughout the whole bulk of resultant CTA membranes.

The *A*, *B*, porosity and S value of resultant CTA FO membranes are shown in Table 6. Obviously, *A* and *B* were much higher than the values reported in other literatures [43,44]. It was due to the elimination of dense bottom and

Table 5
Permeability properties of CTA membranes prepared via in situ interfacial polymerization using non-woven as substrate

Membrane No.	Water flux (J_w, LMH)		Reverse salt flux (J_s, gMH)		J_s/J_w	
	FO	PRO	FO	PRO	FO	PRO
MCTA13-00	6.08 ± 0.33	6.29 ± 0.01	42 ± 10	38 ± 5	6.9	6.04
MCTA13-02	6.58 ± 0.38	6.83 ± 1.98	25 ± 6	21 ± 3	3.80	3.07
MCTA13-04	7.10 ± 0.24	7.87 ± 2.14	24 ± 5	23 ± 5	3.38	2.92
MCTA13-06	7.27 ± 0.13	8.14 ± 2.91	23 ± 6	23 ± 7	3.16	2.83
MCTA13-08	8.27 ± 0.06	8.31 ± 0.04	23 ± 4	20 ± 9	2.02	2.76
MCTA13-10	8.52 ± 0.86	9.02 ± 1.55	21 ± 12	23 ± 9	2.25	2.55
MCTA13-100	8.20 ± 0.82	9.66 ± 1.33	18 ± 6	20 ± 6	2.5	2.07

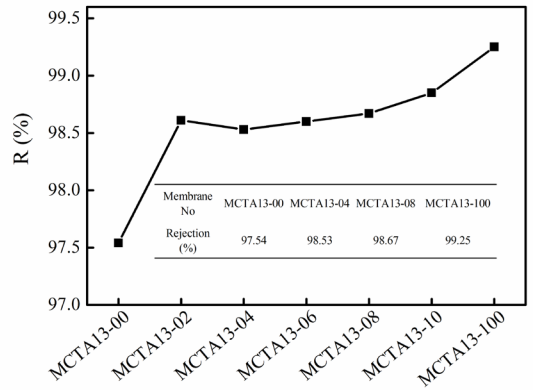

Fig. 8. FO rejection of NaCl of CTA membranes prepared via in situ interfacial polymerization using non-woven as substrate.

Table 6
The porosity, *A*, *B* and *S* values of CTA membranes prepared via in situ interfacial polymerization using non-woven as substrate

Membrane No.	Water permeability (*A*, LMH/Bar)	Salt permeability (*B*, LMH)	Porosity (%)	*S* (mm)
MCTA13-00	244 ± 15	53.36	68 ± 0.29	4.96
MCTA13-04	235 ± 23	13.79	62 ± 0.15	4.93
MCTA13-08	226 ± 17	13.06	60 ± 0.71	4.68
MCTA13-10	208 ± 8	13.86	53 ± 1.31	4.22
MCTA13-100	200 ± 15	12.69	49 ± 2.24	3.97

top layer. Besides, both *A* and *B* decreased when MPD concentration increased in the coagulation bath. The *B* value of MCTA13-00 was much higher than that using MPD solution as coagulation bath. It was attributed to the polyamide layer formed in the demixing process. It was notable that the porosity of membrane MCTA13-00 was higher than that using MPD solution as coagulation bath. The much higher porosity was owing to the macrovoids in the membrane that could be observed from the SEM image. Besides, the porosity decreased remarkably as MPD concentration increased in the coagulation. However, the *S* decreased as well with the improvement of MPD concentration in the coagulants. In general, higher porosity was conductive to decrease *S* [45]. However, *S* decreased though porosity decreased. The decreased *S* indicated the ICP being mitigated. The reason was that the polyamide selective layer prevented the salt diffusion into the porous layer thus alleviating the ICP. This was quite in accordance with the membranes FO performance.

4. Conclusion

The CTA flat-sheet FO membranes were prepared on the non-woven substrate by the in situ polymerization method. TMC in the casting solution reacted with the MPD in the coagulation bath to form the polyamide selective layer synchronous during the precipitation process. The active layer was formed not only on the both top and bottom surface but also throughout whole bulk of resultant CTA FO membrane. And the selective layer enhanced with increasing concentration of MPD in the coagulants. Furthermore, the non-woven substrate and the in situ polymerization method resulted in decreasing *S* with increasing MPD concentration in the coagulant. This explained that FO permeability properties were improved in terms of increasing water flux and decreasing reverse salt flux when MPD concentration increased. Besides, the selective layer throughout the whole bulk of CTA FO membrane prevented the salt diffusing into the porous layer. Therefore, the ICP was effectively alleviated. This resulted in the tiny performance differences between FO mode and PRO mode.

Acknowledgments

The authors gratefully acknowledge the National Science and Technology Support Project of China (2014BAB07B01 and 2015BAB09B01), the China Postdoctoral Science Foundation (2015M571513), 2013 Year Special Project of the Development and Industrialization of New Materials of National Development and Reform Commission in China (GX1301) and the Key Technology R&D Program of Jiangsu Committee of Science and Technology in China (BE2013031).

References

[1] R.L. McGinnis, M. Elimelech, Global challenges in energy and water supply: the promise of engineered osmosis, Environ. Sci. Technol., 42 (2008) 8625–8629.

[2] Y. Matsuo, A. Yanagisawa, Y. Yamashita, A global energy outlook to 2035 with strategic considerations for Asia and Middle East energy supply and demand interdependencies, Energy Strategy Rev., 2 (2013) 79–91.
[3] Y. Chang, J. Lee, H. Yoon, Alternative projection of the world energy consumption-in comparison with the 2010 international energy outlook, Energy Policy, 50 (2012) 154–160.
[4] S. Zhu, M. Li, M. Gamal El-Din, Forward osmosis as an approach to manage oil sands tailings water and on-site basal depressurization water, J. Hazard. Mater., 327 (2017) 18–27.
[5] E.A. Bell, T.E. Poynor, K.B. Newhart, Produced water treatment using forward osmosis membranes: evaluation of extended-time performance and fouling, J. Membr. Sci., 525 (2017) 77–88.
[6] W. Xu, J.-g. Sun, M. Chen, Forward osmosis application in tomato juice processing, Food Ferment. Ind., 39 (2013) 128–130.
[7] S. Phuntsho, S. Hong, M. Elimelech, Forward osmosis desalination of brackish groundwater: meeting water quality requirements for fertigation by integrating nanofiltration, J. Membr. Sci., 436 (2013) 1–15.
[8] B.D. Coday, N. Almaraz, T.Y. Cath, Forward osmosis desalination of oil and gas wastewater: impacts of membrane selection and operating conditions on process performance, J. Membr. Sci., 488 (2015) 40–55.
[9] T.-S. Chung, S. Zhang, K.Y. Wang, Forward osmosis processes: yesterday, today and tomorrow, Desalination, 287 (2012) 78–81.
[10] T.Y. Cath, A.E. Childress, M. Elimelech, Forward osmosis: principles, applications, and recent developments, J. Membr. Sci., 281 (2006) 70–87.
[11] D.L. Shaffer, J.R. Werber, H. Jaramillo, Forward osmosis: where are we now? Desalination, 356 (2015) 271–284.
[12] M. Sairam, E. Sereewatthanawut, K. Li, Method for the preparation of cellulose acetate flat sheet composite membranes for forward osmosis—desalination using $MgSO_4$ draw solution, Desalination, 273 (2011) 299–307.
[13] S. Zhang, K.Y. Wang, T.-S. Chung, Molecular design of the cellulose ester-based forward osmosis membranes for desalination, Chem. Eng. Sci., 66 (2011) 2008–2018.
[14] T.P.N. Nguyen, E.-T. Yun, I.-C. Kim, Preparation of cellulose triacetate/cellulose acetate (CTA/CA)-based membranes for forward osmosis, J. Membr. Sci., 433 (2013) 49–59.
[15] S. Zhang, K.Y. Wang, T.-S. Chung, Well-constructed cellulose acetate membranes for forward osmosis: minimized internal concentration polarization with an ultra-thin selective layer, J. Membr. Sci., 360 (2010) 522–535.
[16] H. El-Saied, A.H. Basta, B.N. Barsoum, Cellulose membranes for reverse osmosis Part I. RO cellulose acetate membranes including a composite with polypropylene, Desalination, 159 (2003) 171–181.
[17] A. Ahmad, S. Waheed, S.M. Khan, Effect of silica on the properties of cellulose acetate/polyethylene glycol membranes for reverse osmosis, Desalination, 355 (2015) 1–10.
[18] T.-Y. Liu, C.-K. Li, B. Pang, Fabrication of a dual-layer (CA/PVDF) hollow fiber membrane for RO concentrate treatment, Desalination, 365 (2015) 57–69.
[19] G. Sabad-e, S. Waheed, A. Ahmad, S.M. Khan, M. Hussain, T. Jamil, M. Zuber, Synthesis, characterization and permeation performance of cellulose acetate/polyethylene glycol-600 membranes loaded with silver particles for ultra low pressure reverse osmosis, J. Taiwan Inst. Chem. Eng., 57 (2015) 129–138.
[20] C.M. Kee, A. Idris, Permeability performance of different molecular weight cellulose acetate hemodialysis membrane, Sep. Purif. Technol., 75 (2010) 102–113.
[21] S.M. Hosseini, A. Gholami, S.S. Madaeni, Fabrication of (polyvinyl chloride/cellulose acetate) electrodialysis heterogeneous cation exchange membrane: Characterization and performance in desalination process, Desalination, 306 (2012) 51–59.
[22] A. Idris, L.K. Yet, The effect of different molecular weight PEG additives on cellulose acetate asymmetric dialysis membrane performance, J. Membr. Sci., 280 (2006) 920–927.
[23] J. Su, Q. Yang, J.F. Teo, Cellulose acetate nanofiltration hollow fiber membranes for forward osmosis processes, J. Membr. Sci., 355 (2010) 36–44.
[24] J. Dasgupta, S. Chakraborty, J. Sikder, The effects of thermally stable titanium silicon oxide nanoparticles on structure and performance of cellulose acetate ultrafiltration membranes, Sep. Purif. Technol., 133 (2014) 55–68.
[25] G. Li, X.-M. Li, T. He, Cellulose triacetate forward osmosis membranes: preparation and characterization, Desal. Wat. Treat., 51 (2013) 2656–2665.
[26] K.Y. Wang, R.C. Ong, T.-S. Chung, Double-skinned forward osmosis membranes for reducing internal concentration polarization within the porous sublayer, Ind. Eng. Chem. Res., 49 (2010) 4824–4831.
[27] R.C. Ong, T.S. Chung, Fabrication and positron annihilation spectroscopy (PAS) characterization of cellulose triacetate membranes for forward osmosis, J. Membr. Sci., 394 (2012) 230–240.
[28] N.Y. Yip, A. Tiraferri, W.A. Phillip, High performance thin-film composite forward osmosis membrane, Environ. Sci. Technol., 44 (2010) 3812–3818.
[29] Z. Wang, J. Tang, C. Zhu, Chemical cleaning protocols for thin film composite (TFC) polyamide forward osmosis membranes used for municipal wastewater treatment, J. Membr. Sci., 475 (2015) 184–192.
[30] Z. Zhou, J.Y. Lee, T.-S. Chung, Thin film composite forward-osmosis membranes with enhanced internal osmotic pressure for internal concentration polarization reduction, Chem. Eng. J., 249 (2014) 236–245.
[31] R.C. Ong, T.-S. Chung, J.S. de Wit, Novel cellulose ester substrates for high performance flat-sheet thin-film composite (TFC) forward osmosis (FO) membranes, J. Membr. Sci., 473 (2015) 63–71.
[32] K.Y. Wang, T.-S. Chung, G. Amy, Developing thin-film-composite forward osmosis membranes on the PES/SPSf substrate through interfacial polymerization, AIChE J., 58 (2012) 770–781.
[33] J. Su, T.S. Chung, Sublayer structure and reflection coefficient and their effects on concentration polarization and membrane performance in FO processes, J. Membr. Sci., 376 (2011) 214–224.
[34] Z. Dabaghian, A. Rahimpour, Carboxylated carbon nanofibers as hydrophilic porous material to modification of cellulosic membranes for forward osmosis desalination, Chem. Eng. Res. Des., 104 (2015) 647–657.
[35] J.M.C. Puguan, H.-S. Kim, K.-J. Lee, Low internal concentration polarization in forward osmosis membranes with hydrophilic crosslinked PVA nanofibers as porous support layer, Desalination, 336 (2014) 24–31.
[36] E.L. Tian, H. Zhou, Y.W. Ren, Novel design of hydrophobic/hydrophilic interpenetrating network composite nanofibers for the support layer of forward osmosis membrane, Desalination, 347 (2014) 207–214.
[37] L. Huang, J.T. Arena, J.R. McCutcheon, Surface modified PVDF nanofiber supported thin film composite membranes for forward osmosis, J. Membr. Sci., 499 (2016) 352–360.
[38] M. Shibuya, M. Yasukawa, S. Goda, Experimental and theoretical study of a forward osmosis hollow fiber membrane module with a cross-wound configuration, J. Membr. Sci., 504 (2016) 10–19.
[39] Z. Dabaghian, A. Rahimpour, M. Jahanshahi, Highly porous cellulosic nanocomposite membranes with enhanced performance for forward osmosis desalination, Desalination, 381 (2016) 117–125.
[40] P. Lu, S. Liang, T. Zhou, Typical thin-film composite (TFC) membranes modified with inorganic nanomaterials for forward osmosis: a review, Nanosci. Nanotechnol. Lett., 8 (2016) 906–916.
[41] Y. Wang, R. Ou, Q. Ge, Preparation of polyethersulfone/carbon nanotube substrate for high-performance forward osmosis membrane, Desalination, 330 (2013) 70–78.
[42] M. Obaid, Z.K. Ghouri, O.A. Fadali, Amorphous SiO_2 NP-incorporated poly(vinylidene fluoride) electrospun

nanofiber membrane for high flux forward osmosis desalination, ACS Appl. Mater. Interfaces, 8 (2016) 4561–4574.
[43] X. Li, K.Y. Wang, B. Helmer, Thin-film composite membranes and formation mechanism of thin-film layers on hydrophilic cellulose acetate propionate substrates for forward osmosis processes, Ind. Eng. Chem. Res., 51 (2012) 10039–10050.
[44] G. Han, T.-S. Chung, M. Toriida, Thin-film composite forward osmosis membranes with novel hydrophilic supports for desalination, J. Membr. Sci., 423–424 (2012) 543–555.
[45] S. Chou, L. Shi, R. Wang, Characteristics and potential applications of a novel forward osmosis hollow fiber membrane, Desalination, 261 (2010) 365–372.